Systematic study of the (n, 2n) reaction cross section for ^{121}Sb and ^{123}Sb isotopes

R. K. Singh[1†] N. L. Singh[1,2‡] R. D. Chauhan[1] Mayur Mehta[3] S. V. Suryanarayana[4] Rajnikant Makwana[1]
B. K. Nayak[4] H. Naik[5] Tarak Nath Nag[5] K. Katovsky[6]

[1]Department of Physics, Faculty of Science, the M. S. University of Baroda, Vadodara - 390002, INDIA
[2]Department of Physics, Netaji Subhas University of Technology, Dwarka, New Delhi- 110078, INDIA
[3]Institute for Plasma Research, Gandhinagar- 382428, INDIA
[4]Nuclear Physics Division, Bhabha Atomic Research Centre, Mumbai, INDIA
[5]Radiochemistry Division, Bhabha Atomic Research Centre, Mumbai, INDIA
[6]Department of Electrical Power Engineering, Brno University of Technology, Brno-61600, Czech Republic

Abstract: The cross sections of the ^{121}Sb$(n,2n)^{120}$Sb^{m} and ^{123}Sb$(n,2n)^{122}$Sb reactions were measured at 12.50, 15.79 and 18.87 MeV neutron energies relative to the standard ^{27}Al$(n,\alpha)^{24}$Na monitor reaction using neutron activation and offline γ-ray spectrometry. Irradiation of the samples was performed at the BARC-TIFR Pelletron Linac Facility, Mumbai, India. The quasi-monoenergetic neutrons were generated via the ^{7}Li(p,n) reaction. Statistical model calculations were performed by nuclear reaction codes TALYS (ver. 1.9) and EMPIRE (ver. 3.2.2) using various input parameters and nuclear level density models. The cross sections of the ground and the isomeric state as well as the isomeric cross section ratio were studied theoretically from reaction threshold to 26 MeV energies. The effect of pre-equilibrium emission is also discussed in detail using different theoretical models. The present measured cross sections were discussed and compared with the reported experimental data and evaluation data of the JEFF-3.3, ENDF/B-VIII.0, JENDL/AD-2017 and TENDL-2019 libraries. A detailed analysis of the uncertainties in the measured cross section data was performed using the covariance analysis method. Furthermore, a systematic study of the $(n,2n)$ reaction cross section for ^{121}Sb and ^{123}Sb isotopes was also performed within 14–15 MeV neutron energies using various systematic formulae. This work helps to overcome discrepancies in Sb data and illustrate a better understanding of pre-equilibrium emission in the $(n,2n)$ reaction channel.

Keywords: antimony, (n, 2n) reaction cross section, ^{7}Li(p, n) reaction neutron source, neutron activation and offline γ-ray spectrometry, systematic formulae, covariance analysis, TALYS (ver. 1.9) and EMPIRE (ver. 3.2.2) codes

DOI: 10.1088/1674-1137/ac4a5a

I. INTRODUCTION

Nuclear data such as cross section, half-life, decay modes, decay radiation properties, and γ-rays from radionuclides of the various radioisotopes are widely used in nuclear medicine, radiation shielding, fusion/fission reactor design, radioactive waste disposal and transmutation, radiation safety, etc. Neutron-induced reaction cross section data for different nuclei is often used to predict various theoretical nuclear models [1]. The $(n,2n)$ reaction cross sections of the ^{121}Sb and ^{123}Sb isotopes are essential for neutron multiplication calculations. In recent years, the ^{121}Sb$(n,2n)^{120}$Sb and ^{123}Sb$(n,2n)^{122}$Sb reaction cross sections within the energy range 13 to 20 MeV was measured by several authors, as mentioned in the EXFOR compilation [2]. The available experimental and evaluated data of the ^{121}Sb$(n,2n)^{120}$Sb and ^{123}Sb$(n,2n)^{122}$Sb reactions from threshold to 20 MeV shows disagreement at the same incident energy. Since there are significant discrepancies in the measured cross section and evaluated data from different libraries for common incident neutron energy, it is difficult to refine and correct various statistical parameters.

The compound nucleus, direct and pre-equilibrium emission are the different models used to understand the reaction mechanism, and the optimum parameters needed to understand these processes. Therefore, it is essential to improve the accuracy of measured experimental data and understand these reaction models [3]. Some of the anti-

Received 7 May 2021; Accepted 12 January 2022; Published online 18 March 2022
† E-mail: ratankumar339@gmail.com
‡ E-mail: nl.singh-phy@msubaroda.ac.in

mony isotopes in nuclear fission have been identified as nuclides of the fission product. For the decommissioning of light-water nuclear reactors, the cross section data of neutron-induced reactions of antimony are very important. Therefore, fast-neutron-induced cross section measurements with better accuracy for antimony are essential for improving nuclear data [4–5]. It was observed that when antimony is alloyed with lead, this increased the hardness and mechanical strength of lead. This lead–antimony alloy is used in radiation shielding. The ^{123}Sb$(n,2n)^{122}$Sb reaction produces ^{122}Sb ($\tau_{1/2}$ = 2.47 day) nuclei, and essential radiotracers are used to study food crops and environmental contamination. Natural antimony is also used in the start-up of neutron sources [6–7].

The neutron-induced reactions that result in the formation of various isomers of residual nuclei are crucial for better understanding the role of nuclear structure in the compound nucleus reaction process. In comparison with the ground state of ^{120}Sb^{g} and ^{122}Sb^{g} with spin $J^{\pi} = 1^{+}$ and $J^{\pi} = 2^{-}$, ^{120}Sb^{m} and ^{122}Sb^{m} are high spin isomers, each with a spin value of $J^{\pi} = 8^{-}$. Due to the high spin value 8^{-} of the isomeric state relative to the ground state 1^{+} and 2^{-} value, the spin distribution of the residual nucleus can be studied with great sensitivity [8].

In the present work, the excitation functions of the ^{121}Sb$(n,2n)^{120}$Sb^{m} and ^{123}Sb$(n,2n)^{122}$Sb reactions were measured at 12.50, 15.79 and 18.87 MeV neutron energies. The experimental results and latest evaluated data from JEFF-3.3 [9], JENDL/AD-2017 [10], ENDF/B-VIII.0 [11] and TENDL-2019 [12] libraries were compared with the each other. Specifically, the uncertainties in the measured cross section data were obtained through the covariance analysis method, which involves uncertainties from each source. In addition, a systematic study of the $(n,2n)$ reaction cross section for antimony isotopes was also carried out using different formulae given by several authors. The isomeric cross section ratio σ_m/σ_g for the ^{121}Sb$(n,2n)^{120}$Sb^{m,g} and ^{123}Sb$(n,2n)^{122}$Sb^{m,g} reactions were studied theoretically in the energy range 10 –26 MeV using the TALYS (ver. 1.9) [13] and EMPIRE (ver. 3.2.2) [14] codes. The present measurements and available literature data were compared with theoretical calculations performed using the two codes. Additionally, the different theoretical models from the two codes were used to study the pre-equilibrium process mechanism and the contribution to the current interest reaction channels. The main reason for measuring the $(n,2n)$ reaction cross section of ^{121}Sb and ^{123}Sb isotopes was the lack of sufficient data at higher energies.

II. NEUTRON SOURCE

The 6-m elevation level (above analysing magnet) irradiation setup of the 14UD BARC-TIFR Pelletron accelerator facility at Mumbai, India, was used for neutron generation and activation. Quasi-monoenergetic neutrons are produced when a proton beam with current of 150–160 nA is incident on the natural lithium foil through the ^{7}Li(p,n) reaction. The pressure inside the 6-m setup was 8×10^{-8} torr, and in the neutron activation zone was atmospheric. The energy spreads of the proton energy at the height of 6 m were 50–90 keV. In the above experimental setup, protons with energies of 15, 18 and 21 MeV after passing through a beam collimator with a diameter of 6 mm have impinged on 8.0-mg/cm^2 thin natural lithium foil, which was prepared at the TIFR target laboratory. This lithium foil was placed between the two tantalum foils of different thicknesses. The lithium target was pasted on 0.1-mm-thick tantalum foil to stop the proton beam along with a 4.0-mg/cm^2 thick front tantalum foil. The energy losses of the protons in the lithium and tantalum foils were calculated from the Monte Carlo simulation code SRIM [15]. The proton energy loss in the lithium foil is from 264.08 to 167.12 keV, whereas in the tantalum foils, it is from 56.7 to 44.96 keV. The samples for irradiation were kept one at a time at a distance of 2.1 cm from the Ta–Li–Ta stack at 0^{o} with respect to the proton beam direction. The experimental arrangement for the neutron irradiation is shown in Fig. 1.

In the above experimental setup, when the natural lithium foil was bombarded with protons with energies of 15, 18 and 21 MeV, quasi-monoenergetic neutrons (n_0) were produced in the forward direction via the ^{7}Li(p,n) reaction. This reaction ^{7}Li(p,n) ($E_{\rm th}$=1.88 MeV) produces monoenergetic neutrons below the proton energy of 2.4 MeV. However, above the proton energy of 2.4 MeV, the first excited state of ^{7}Be is populated 0.43 MeV above the ground state, which is the second group of neutrons (n_1). The ^{7}Be ground state threshold is 1.881, and neutron energy corresponding to the ground state is E_p−1.881. Similarly, the first excited state threshold for ^{7}Be is 2.38 MeV, and neutron energy corresponding to the first excited state is E_p−2.38. In the ^{7}Li(p,n) reaction, for proton energies below 5 MeV at zero-degree, these low energy neutrons yield less than about 10% of the ground state yield. Thus the usefulness of the monoenergetic neutron source is only slightly impaired. Three-body interactions take place above 6 MeV, which populates excited states of ^{7}Be and produces neutrons with primary neutron peak (n_0) [16]. The primary neutron peak (n_0) has a higher neutron energy and flux, and this peak is used to measure the $(n,2n)$ reaction cross section of antimony isotopes. The neutron distribution for energies of 15, 18 and 21 MeV was obtained by interpolation techniques using the neutron distribution of M. W. Mcnaughton *et al.* [17]. The neutron distribution has a quasi-monoenergetic peak near E_p−1.88 and a long tail towards lower energies, as shown in Fig. 2(a,b,c) for the proton energies of 15, 18 and 21 MeV. This neutron spectrum was used for the neutron energy calculation based on the kinematic rela-

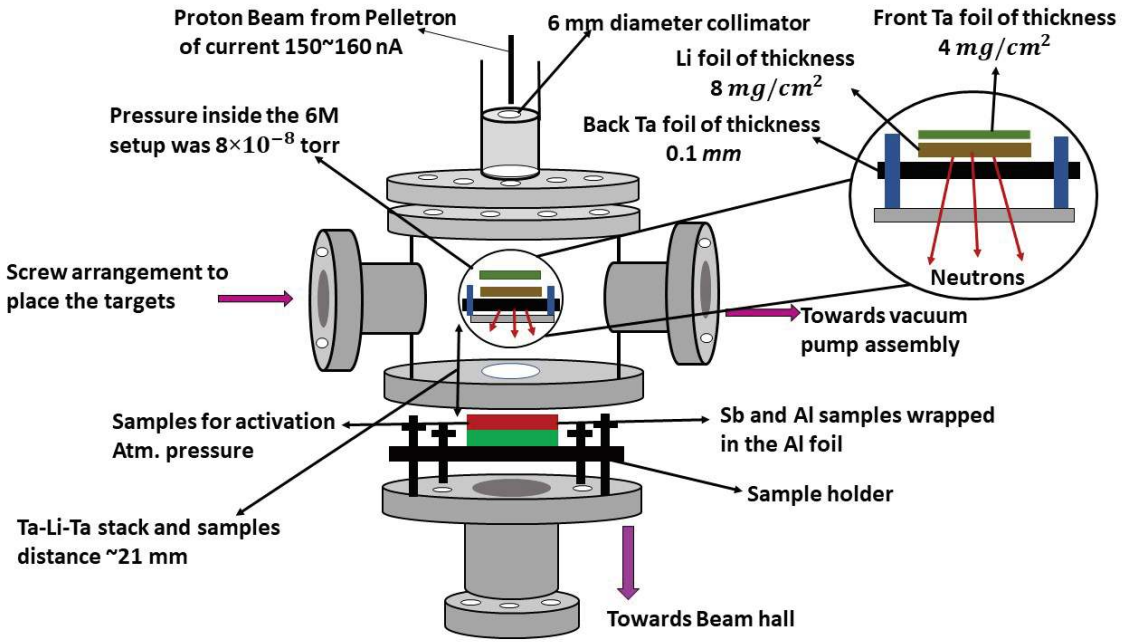

Fig. 1. (color online) Schematic diagram of the experimental setup used for neutron irradiation.

tion $\left(E_n = E_p - E_{\rm th}\right), E_p$ is the proton energy, and $E_{\rm th}$ is the threshold energy of the ^{7}Li(p,n) reaction. The effective mean neutron energy of the primary neutron group from the neutron spectrum was calculated using equation (1), and the uncertainty associated with this neutron energy is the spectrum width of the primary neutron peak. The calculated neutron energy is given as 12.50±0.68, 15.79±0.55 and 18.87±0.59 MeV corresponding to proton energies 15, 18 and 21 MeV.

$$\langle E_n \rangle = \frac{\int_{E_{ps}}^{E_{\rm max}} E_i \phi_i(E)\,{\rm d}E}{\int_{E_{ps}}^{E_{\rm max}} \phi_i(E)\,{\rm d}E}, \qquad (1)$$

$\langle E_n \rangle$ is the effective mean neutron energy, $E_{\rm max}$ is the maximum neutron energy, E_{ps} is the peak forming start energy, E_i is the energy bin and $\phi_i(E)$ is the neutron flux for the energy bin E_i.

III. SAMPLE PREPARATION AND γ–RAY ACTIVITY MEASUREMENTS

A. Sample preparation

Natural antimony (with purity 99.89%) in powder form was used for sample preparation of weight ~600 mg for each sample. Three antimony pellets of area 1.327 cm^2 and diameter 1.3 cm were prepared into circular shapes using the pelletizer. Thin aluminium metal foil (with purity 99.97%) of weight ~25.6 mg was used as a standard for normalization during the irradiation process. The aluminium monitor foil in a square shape of area 1 cm^2 and thickness 0.1 mm was placed with each antimony sample. The neutron flux was determined using the standard ^{27}Al(n,α)^{24}Na reference reaction. During the irradiations, these samples were wrapped in 0.011-mm-thick aluminium foil to prevent radioactive contamination from one another and to the surrounding.

B. γ–ray activity measurements

The samples were irradiated at a distance of 2.1 cm from the neutron source for 7 to 9 hours to obtain sufficient activity in the antimony targets and the reference foils. After the irradiation process and sufficient cooling, the samples were transferred to the low-background counting location. The irradiation, cooling and counting time of the samples at different energies are summarized in Table 1. The emitted γ-rays from the neutron-irradiated samples were measured by a 40% relative efficiency pre-calibrated Baltic p-type coaxial high-purity germanium detector (HPGe) coupled to a PC-based 4096 multichannel analyzer. This detector was shielded with lead blocks to reduce the contribution of the natural background radioactivity. The samples were kept at a distance of 3 cm from the end cup of the HPGe detector to maintain a very low dead time throughout the experiment. At this distance, the correction for the coincident summing effect was considered in the efficiency calculation. The CAMAC-based Genie γ-ray spectroscopy software was used for the data acquisition. The energy and efficiency calibration of the detector was carried out using the standard calibrated ^{152}Eu point source at the same

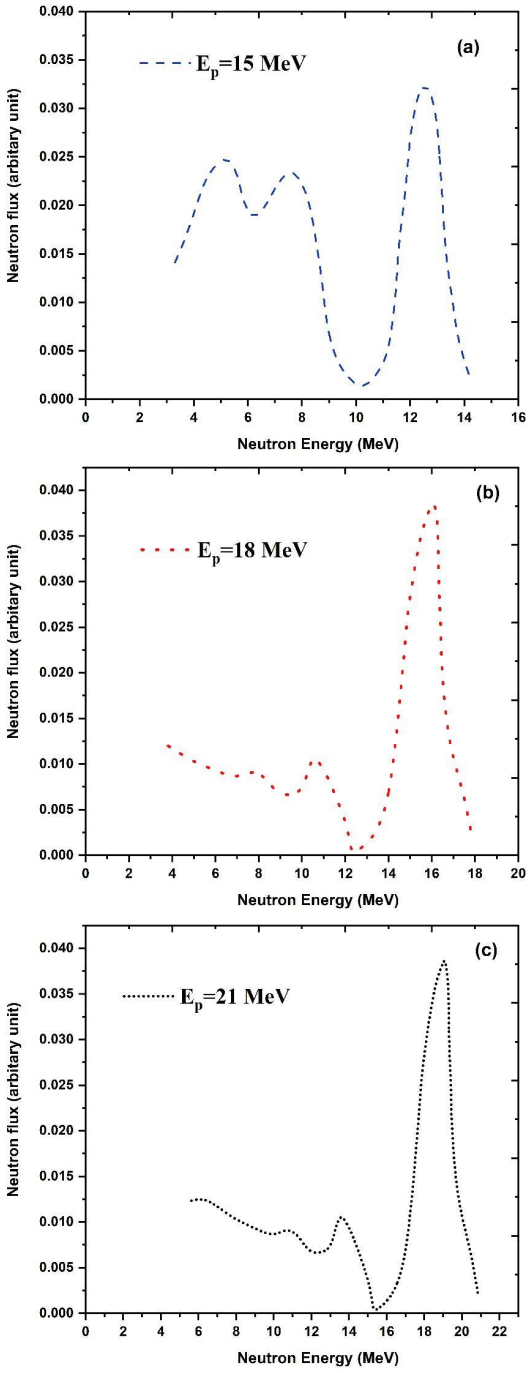

Fig. 2. (color online) Neutron energy flux spectra from the ^{7}Li(p,n) reaction at 0° of the impinging protons at energies 15, 18 and 21 MeV, obtained from the distribution of M. W. Mcnaughton *et al.* [17].

geometry to reduce the coincidence summing effect. The energy resolution of the HPGe detector was 3.305 keV at 1408 keV γ-ray of a standard ^{152}Eu point source. A typical γ-ray spectrum obtained from the HPGe detector is given in Fig. 3, where the 564.12 keV and 1171.3 keV γ-lines of antimony isotopes are seen. The necessary decay data of the antimony and aluminium targets are presented in Table 2.

IV. DATA ANALYSIS AND RESULTS

A. Cross section calculations

The cross sections were measured by irradiating the target samples with a neutrons beam using the neutron activation method. These activated samples emit characteristic γ-rays having a suitable half-life with γ-ray transition probability. The neutron activation cross sections for the selected reactions were calculated relative to the ^{27}Al$(n,\alpha)^{24}$Na reference reaction cross section using the following formula,

$$\langle\sigma_{\rm Sb}\rangle = \langle\sigma_{\rm Al}\rangle \cdot \frac{\left(\varepsilon.I_{\gamma}.Abu.Wt.f\right)_{\rm Al}}{\left(\varepsilon.I_{\gamma}.Abu.Wt.f\right)_{\rm Sb}} \cdot \frac{\left(C.\lambda.AM.\frac{CL}{LT}\right)_{\rm Sb}}{\left(C.\lambda.AM.\frac{CL}{LT}\right)_{\rm Al}} \cdot \prod \frac{C_{\Gamma_{\rm attn}{\rm Sb}} * C_{\rm low Sb} * C_{\rm area Sb}}{C_{\Gamma_{\rm attn}{\rm Al}} * C_{\rm low Al} * C_{\rm area Al}}, \quad (2)$$

where $\sigma_{\rm Sb}$ and $\sigma_{\rm Al}$ are sample and monitor reaction cross sections, C is the γ-ray peak count, λ is the decay constant, ε is the efficiency for the characteristic γ-ray of the radionuclide, I_r is the γ-ray abundance, *Wt.* is the weight, *Abu.* is the isotopic abundance, *AM* is the atomic mass, f is the time factor, CL and LT are the clock and live time, $C_{\rm low}$ is the correction factor due to the low energy neutron contribution, $C_{\Gamma_{\rm attn}}$ is the correction factor due to the self-attenuation of the γ-ray and $C_{\rm area}$ is the correction factor due to area. The following relation gives the time factor f,

$$f = (1-{\rm e}^{-\lambda t_{\rm irr}}).\left(1-{\rm e}^{-\lambda t_{\rm c}}\right).{\rm e}^{-\lambda t_{\rm cool}} \quad (3)$$

where $t_{\rm irr}$ is the irradiation time, $t_{\rm cool}$ is the cooling time and $t_{\rm c}$ is the counting time. The half-life, isotopic abund-

Table 1. Sample details and irradiation, cooling and counting times for Sb samples.

Isotope	Natural abundance (%)	E_p (MeV)	Samples weight (mg)		Thickness (cm)		Irradiation time (sec)	Cooling time (sec)	Counting time (sec)
			Sb pellet	Al foil	Sb pellet	Al foil			
^{121}Sb	57.38 (5)	15	601	25.6	0.07	0.01	32700	20986	1930
^{123}Sb	42.64 (5)	18	602	25.9	0.07	0.01	25200	21475	1244
^{27}Al	100	21	600	25.9	0.07	0.01	25200	24117	1214

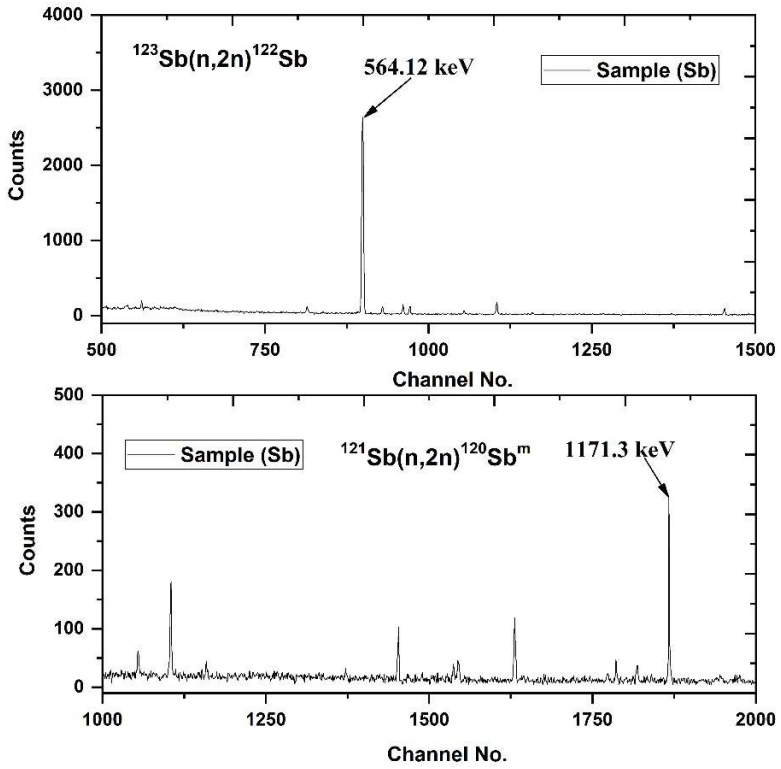

Fig. 3. Typical offline γ-ray energy spectra obtained with an HPGe detector after irradiation at neutron energy of 15.79 MeV for the ^{nat}Sb sample.

Table 2. Nuclear spectroscopic decay data with their uncertainties for sample and monitor reactions [18–20].

Reaction	E_{th}(MeV)	Half-life ($\tau_{1/2}$)	Decay mode	E_γ(keV)	I_γ(%)
^{121}Sb$(n,2n)^{120}$Sb^{m}	9.33	5.76 (2) day	ε(100 %)	1171.3	100
^{123}Sb$(n,2n)^{122}$Sb	9.03	2.72 (2) day	β^- (97.59 %) ε (2.41%)	564.12	70.68 (18)
^{27}Al$(n,\alpha)^{24}$Na	3.47	14.99 (12) hours	β^- (100 %)	1368.62	99.99 (4)

ance, γ-ray abundance and decay mode for the sample and monitor reaction products with their uncertainties are given in Table 2. The spectroscopic decay data with uncertainties were taken from the nuclear database [18–20]. The present measured cross sections of the ^{121}Sb$(n,2n)^{120}$Sb^{m} and ^{123}Sb$(n,2n)^{122}$Sb reactions are given in Table 3.

Interaction of the γ-rays with samples requires correction for the self-attenuation effect. This self-attenuation factor $\Gamma_{\rm attn}$ for activated materials was calculated by the relation $\Gamma_{\rm attn} = ((1-{\rm e}^{-\mu l})/\mu l)$, where l is the thickness of the sample and μ is the mass attenuation coefficient, which was taken from the XMuDat ver.1.0.1 [21–22]. The values for the correction factor of the self-attenuation are given in Table 4. The reaction cross sections were measured for the primary neutron (n_0) energy peak, as shown in Fig. 2. The following relation gives a correction for the low energy background neutrons,

$$C_{\rm low} = 1 - \frac{\int \phi\left(E_{p_1}\right)\sigma_i\left(E_{p_1}\right)}{\int \phi(E)\sigma_i(E){\rm d}E}, \quad (4)$$

where $\phi(E) = \phi\left(E_{p_1}\right) + \phi\left(E_{p_2}\right)$ is the neutron flux, E_{p_1} and E_{p_2} are the primary and secondary neutron energy peaks in the neutron spectrum and $\sigma_i(E)$ is the reaction cross section. The values of this cross section $\sigma_i(E)$ for the sample and monitor reactions were obtained from the TENDL-2019 and IRDFF-1.05 evaluated data libraries [12, 23]. The spectral indexing method for correcting the low energy background neutron is given in Ref. [24]. The calculated values of the correction factor for the low energy background neutrons are given in Table 4. The spectrum-averaged cross section for the monitor reaction is $\langle\sigma_m\rangle$, obtained by the following relation,

$$\langle\sigma_m\rangle = \int \varphi_0\sigma_m(E){\rm d}E \Big/ \int \varphi_0 {\rm d}E. \quad (5)$$

The correlation coefficients for the monitor reaction are obtained using the following equation,

$${\rm Cor}\left(\langle\sigma_i\rangle\langle\sigma_j\rangle\right) = {\rm Cov}\left(\langle\sigma_i\rangle\langle\sigma_j\rangle\right)/(Var\langle\sigma_i\rangle.Var\langle\sigma_j\rangle)^{1/2}. \quad (6)$$

Table 3. Measured cross sections with uncertainties and correlation matrix at E_n =12.50, 15.79 and 18.87 MeV.

$\langle E_n \rangle$ (MeV)	^{121}Sb$(n,2n)^{120}$Sb^{m} (mb)	^{123}Sb$(n,2n)^{122}$Sb (mb)	Correlation matrix
12.50±0.68	424.47±46.35	1371.74±130.56	1.0
15.79±0.55	596.25±94.37	1570.29±233.34	0.1735 1.0
			0.3176 0.2556 1.0
18.87±0.59	633.68±55.17	1412.50±101.63	0.8483 0.1775 0.3233 1.0
			0.1652 0.9253 0.2561 0.1778 1.0
			0.3412 0.2401 0.8511 0.3672 0.2418 1.0

Table 4. Values of γ-ray self-attenuation and low energy background neutron correction factors used to measure the cross section.

Reaction	$\langle E_n \rangle$ (MeV)	E_γ (keV)	$(C_{\Gamma_{\rm attn}})$	$(C_{\rm low})$
^{121}Sb$(n,2n)^{120}$Sb^{m}	12.50	1171.2	0.988029	0.99948
	15.79		0.988064	0.96515
	18.87		0.988076	0.90076
^{123}Sb$(n,2n)^{122}$Sb	12.50	564.2	0.980661	0.99841
	15.79		0.980717	0.95577
	18.87		0.980736	0.88616
^{27}Al$(n,\alpha)^{24}$Na	12.50	1368.62	0.999322	0.87381
	15.79		0.999330	0.90274
	18.87		0.999320	0.75953

The reference cross section of the ^{27}Al$(n,\alpha)^{24}$Na monitor reaction at the nearest point energies was calculated using the evaluated cross-section data of the IRDFF-1.05 [23] library. The monitor cross sections with uncertainties and the covariance and correlation matrix are given in Table 5.

B. Covariance analysis

We calculated the covariance matrix for the detector efficiency and reaction cross section in the above data analysis. All the uncertainty information for the experimental data is included in the covariance matrix. Therefore, the calculated matrix gives complete information of the uncertainties in the measured cross section. The efficiencies of the detector were measured using γ-lines of the calibrated ^{152}Eu point source. The following relation gives the efficiency of the HPGe detector,

$$\varepsilon = \frac{CK_c}{N_0 I_\gamma e^{-\lambda t}}, \tag{7}$$

where ε is the efficiency of the corresponding γ-rays, C is the count under the gamma peak, N_0 is the activity of the standard ^{152}Eu source at an initial time, I_γ is the γ-ray intensity, λ is the decay constant of ^{152}Eu, K_C is the correction factor for the coincidence summing effect, and t is the time elapsed from the manufacture date to the start of counting. The correction factor K_C was calculated from the Monte Carlo Simulation code EFFTRAN [25] using HPGe detector structured data such as crystal hole cavity, end cup, mount cup, crystal material, dimension, absorber, window and calibration source information. It is observed that the HPGe detector efficiency is the function of counts, decay constant, the activity of source and γ-ray intensity. Uncertainty in these four variables propagates in the detector efficiency estimation. Therefore, detector efficiency can be written as the function of only four attributes, $I_\gamma, \lambda, C, N_0$. The total uncertainties due to these four attributes in detector efficiency were calculated using quadratic sum formula,

$$\left(\frac{\Delta\varepsilon_i}{\varepsilon_i}\right)^2 = \left(\frac{\Delta C_i}{C_i}\right)^2 + \left(\frac{\Delta I_{\gamma i}}{I_{\gamma i}}\right)^2 + \left(\frac{\Delta N_0}{N_0}\right)^2 + (t\Delta\lambda)^2. \tag{8}$$

Uncertainty in the decay constant is $\Delta\lambda = \left(0.693 * \Delta\tau_{1/2}/\tau_{1/2}^2\right)$.

The knowledge about the partial uncertainties and their correlations provides a foundation for creating the covariance matrix, which fully describes the uncertainties in the calculated efficiencies. It is possible to directly calculate the elements of this covariance matrix using the formula,

$$(V_\varepsilon)_{ij} = \sum\nolimits_r e_{ir} S_{ijr} e_{jr}, \tag{9}$$

where S_{ijr} is the $n \times n$ micro-correlation matrix between the $i^{\rm th}$ and $j^{\rm th}$ observations due to the $r^{\rm th}$ attributes, e_{ir}

Table 5. Standard ^{27}Al$(n,\alpha)^{24}$Na reaction cross sections with their covariance and correlation matrix obtained from IRDFF-1.05 [23].

$\langle E_n \rangle$ (MeV)	Cross section (mb)	Covariance matrix	Correlation matrix
12.50±0.68	118.94±0.079	0.006326	1.0
15.79±0.55	114.38±0.067	0.000389 0.004493	0.0729 1.0
18.87±0.59	55.74±0.108	0.002165 0.000917 0.01168	0.2517 0.1265 1.0

and e_{jr} are the $n\times n$ diagonal matrices of partial uncertainties of the i^{th} and j^{th} observations due to the r^{th} attributes. The partial uncertainties in different attributes are given in Table 6. The total error in the measured efficiencies is related to the variances by the formula $\sigma_{\varepsilon ii}=((V_{\varepsilon})_{ii})^{1/2}$. The calculated covariance and correlation matrix for the HPGe detector efficiency is given in Table 7. The γ-rays emitted by ^{120}Sb^{m}, ^{122}Sb and ^{24}Na nuclei are different from the γ-ray of the standard ^{152}Eu source. A linear interpolation method was used in the calculation to estimate efficiencies for the corresponding γ-rays of ^{120}Sb^{m}, ^{122}Sb and ^{24}Na nuclei. An empirical relation as a model through interpolation uses the following linear parametric function,

$$\ln(\varepsilon_i)=\sum_{k=1}^{m}p_k(\ln[E_i])^{k-1}, \tag{10}$$

where ε_i is the efficiency for the corresponding γ-ray energy, E_i and p_k is the fitting parameter. The least-square condition states that the best estimate for $\grave{P}$ in the model is the one that minimizes the chi-square statistic given by $\chi^2_m=(Z-AP)^{'}V_Z^{-1}(Z-AP)$. From the least square method, the best estimate for $\grave{P}$ is calculated by the following relation,

$$\grave{P}=\left(A^TV_z^{-1}A\right)^{-1}\left(A^TV_z^{-1}Z\right). \tag{11}$$

In the above equation $\grave{P}$ is the column matrix, V_z was calculated as $(V_{\varepsilon})_{ij}/\varepsilon_i\varepsilon_j$ where V_{ε} is the covariance matrix for the corresponding efficiencies ε, A is the design matrix with $A_{ik}=(\ln[E_i])^{k-1}$, k = 1, 2... 7, i = 1, 2... 8 and Z is the column matrix with $Z_i=\ln(\varepsilon_i)$ [26]. The best fit of the chosen model in the present work was obtained by considering six parameters, and the model gives the best fit value for k=7 and i=8, with the goodness of fit χ^2 =0.799. We consider the following linear parametric model as the best model, which gives the values of fitting parameters $\grave{P}$ =−5.453, −1.092, 1.783, −0.0567, −5.579, −4.976, −1.208. From the above calculation, the correlation matrix and efficiencies for the characteristics γ-rays of the ^{120}Sb^{m}, ^{122}Sb and ^{24}Na are given in Table 8.

In covariance analysis, a ratio method was used for the calculation of the activation cross section. In the standard equation (2), the sample reaction cross section was normalized to monitor the reaction cross section. We obtained the ratio of $\langle\sigma_r\rangle$ and $\langle\sigma_m\rangle$, i.e. the sample and monitor reaction cross sections. The covariance matrix for the measured cross section was calculated by the following formula,

$$(V_{\sigma s})_{ij}=\sum_r e_{ir}S_{ijr}e_{jr}, \tag{12}$$

where S_{ijr} is the $n\times n$ micro-correlation matrix between the i^{th} and j^{th} observations due to the r^{th} attributes, e_{ir} and

Table 6. Partial uncertainties in various parameters to obtain HPGe detector efficiency.

E_γ (keV)	Counts(×10^{-4})	Half-life(×10^{-4})	I_γ (×10^{-4})	Activity(×10^{-4})	Total Uncertainty(×10^{-4})
121.78	0.619	2.092	1.331	2.698	3.716
244.69	1.081	1.556	4.434	2.008	5.223
344.27	0.489	1.166	2.001	1.504	2.804
443.96	1.455	1.105	0.623	1.426	2.401
778.91	0.457	0.522	3.665	0.673	3.791
964.08	0.391	0.433	2.359	0.558	1.493
1085.87	0.381	0.358	1.995	0.462	2.114
1408.01	0.261	0.285	1.389	0.368	1.448

Table 7. Calculated covariance and correlation matrix for the HPGe detector efficiencies.

E_γ (keV)	Covariance matrix (×10^{-8})								Correlation matrix							
121.78	13.81								1.0							
244.69	8.672	27.28							0.446	1.0						
344.27	6.497	4.834	7.865						0.623	0.331	1.0					
443.96	6.159	4.852	3.433	5.761					0.691	0.365	0.511	1.0				
778.91	2.906	2.162	1.619	1.535	14.36				0.206	0.109	0.152	0.168	1.0			
964.08	2.411	1.794	1.344	1.274	0.601	6.216			0.261	0.137	0.192	0.213	0.063	1.0		
1085.86	1.966	1.485	1.112	1.054	0.497	0.413	4.466		0.254	0.134	0.187	0.208	0.062	0.078	1.0	
1408.01	1.588	1.182	0.885	0.839	0.396	0.328	0.272	2.214	0.287	0.152	0.212	0.235	0.071	0.089	0.086	1.0

Table 8. Interpolated detector efficiencies of the characteristic γ-rays of the product nuclides with their uncertainties and correlation matrix.

Reaction	Nuclide	E_γ (keV)	Efficiency	Correlation matrix		
^{121}Sb$(n,2n)^{120}$Sb^{m}	^{120}Sb^{m}	1171.2	0.003749±0.0001326	1.0		
^{123}Sb$(n,2n)^{122}$Sb	^{122}Sb	564.2	0.010791±0.0002988	0.4826	1.0	
^{27}Al$(n,\alpha)^{24}$Na	^{24}Na	1368.6	0.003369±0.0001385	0.6459	0.1056	1.0

e_{jr} are the $n\times n$ diagonal matrix of partial uncertainty i^{th} and j^{th} observations due to the r^{th} attributes [27]. The Table 9 summarizes the partial uncertainties in various parameters to obtain$(n,2n)$ reaction cross section of Sb isotopes. The calculated correlation matrix for the ^{121}Sb$(n,2n)^{120}$Sb^{m} and ^{123}Sb$(n,2n)^{122}$Sb reactions cross sections is given in Table 9. The error in the measured cross sections are calculated by taking the square root of the diagonal elements of the covariance matrix, i.e. $((V_{\sigma s})_{ii})^{1/2}$. The source of uncertainty and their values in the present measured cross sections are given as follows: counting statistics (≤5%), isotopic abundance (≤1%), detector efficiency (≤4%), the weight of samples (≤0.01%), reference cross section (≤1%), and self-absorption of γ-ray (≤1%). The uncertainties due to the other sources are very small and neglected in measured cross sections.

C. Experimental results

There are no evaluation cross sections in the database of IAEA for the ^{121}Sb$(n,2n)^{120}$Sb^{m}, ^{121}Sb$(n,2n)^{120}$Sb^{g}, ^{123}Sb$(n,2n)^{122}$Sb^{m} and ^{123}Sb$(n,2n)^{122}$Sb^{g} reactions. The results of the present measurements with cross sections at neutron energies of 12.50, 15.79 and 18.87 MeV are plotted in Figs. 4(a) and 5(c) along with all other reported data. We can see from Figs. 4(c) and 5(c) that the trends of these evaluation excitation curves of JEFF-3.3, TENDL-2019, JENDL/AD-2017 and ENDF/B-VIII.0 are not the same.

For the isomeric state cross section from Fig. 4(a), our results are higher than those obtained by N. L. Das *et al.* [54], W. D. Lu *et al.* [55] and A. Reggoug *et al.* [66]. At 15.79 and 18.87 MeV, the present measured data are in agreement with the results of S. K. Ghorai *et al.* [56] and M. Bormann *et al.* [59] within experimental uncertainties. In contrast, at 12.50 MeV, the present data lies between the data of S. K. Ghorai *et al.* [56] and Y. Kanda [65]. In addition, for the isomeric state the cross section values of J. L Casanova [62] is much higher than the present measured cross section. Similarly, the reported measurements of the various experiments for the ^{121}Sb$(n,2n)^{120}$Sb^{g} reaction agree very well except for some of the reported data by R. A. Jarjis [60] and C. Carles [69] as shown in Fig. 4(b).

It can be seen from Fig. 4(c) that in the 14 to 20 MeV energy range, results of N. L. Das *et al.* [54], M. Bormann *et al.* [59] and Y. Kanda [65] are consistent with the result of ENDF/B-VIII.0 evaluation for the

Table 9. Partial uncertainties in various parameters to obtain the ^{121}Sb$(n,2n)^{120}$Sb^{m} and ^{123}Sb$(n,2n)^{122}$Sb reactions cross section.

Parameters	^{121}Sb$(n,2n)^{120}$Sb^{m}			^{123}Sb$(n,2n)^{122}$Sb		
	$\langle E_n\rangle$=12.50 (MeV)	$\langle E_n\rangle$=15.79 (MeV)	$\langle E_n\rangle$=18.87 (MeV)	$\langle E_n\rangle$=12.50 (MeV)	$\langle E_n\rangle$=15.79 (MeV)	$\langle E_n\rangle$=18.87 (MeV)
σ_{Al}	2.838	3.498	12.289	9.172	9.218	2.740
C_{Sb}	22.657	32.923	17.691	23.466	28.323	15.095
AM_{Sb}	0.070	0.099	0.105	0.112	0.128	0.115
λ_{Sb}	2.963	4.232	5.993	9.353	10.802	9.289
W_{Al}	6.367	11.925	15.842	27.435	39.282	3.533
$I\gamma_{Al}$	0.170	0.239	0.253	0.549	0.629	0.565
ε_{Al}	17.450	24.512	26.051	56.392	64.596	58.090
C_{Al}	31.208	77.626	31.804	100.852	204.565	70.918
AM_{Al}	0.472	0.663	0.705	1.525	1.747	1.571
λ_{Al}	1.117	2.063	3.128	3.608	5.438	6.684
W_{Sb}	8.504	23.850	9.505	27.480	62.852	2.120
$Abun_{Sb}$	0.212	0.298	0.317	0.683	0.782	0.703
$I\gamma_{Sb}$	0.006	0.009	0.010	2.465	2.823	2.539
ε_{Sb}	15.010	21.085	22.408	37.983	43.509	39.127

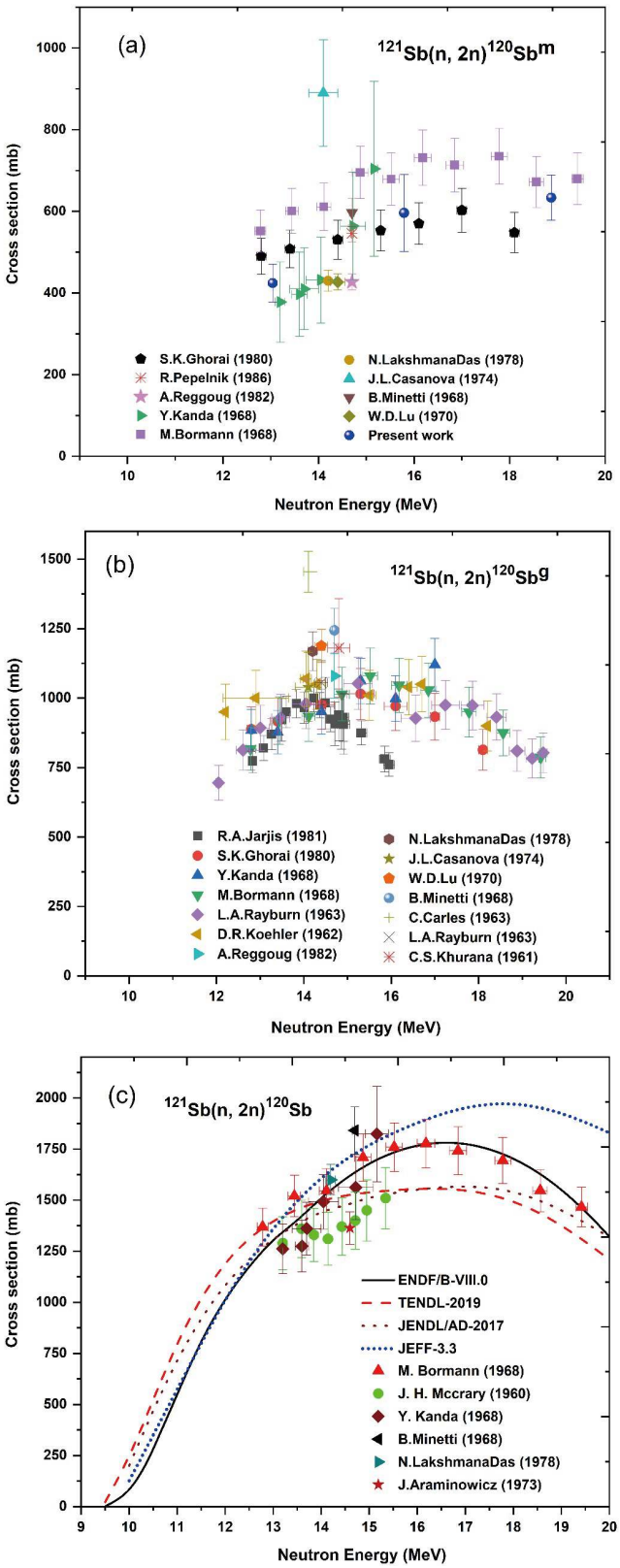

Fig. 4. (color online) Comparison of existing literature and evaluated data of the ^{121}Sb$(n,2n)^{120}$Sb^{m}, ^{121}Sb$(n,2n)^{120}$Sb^{g} and ^{121}Sb$(n,2n)^{120}$Sb reactions.

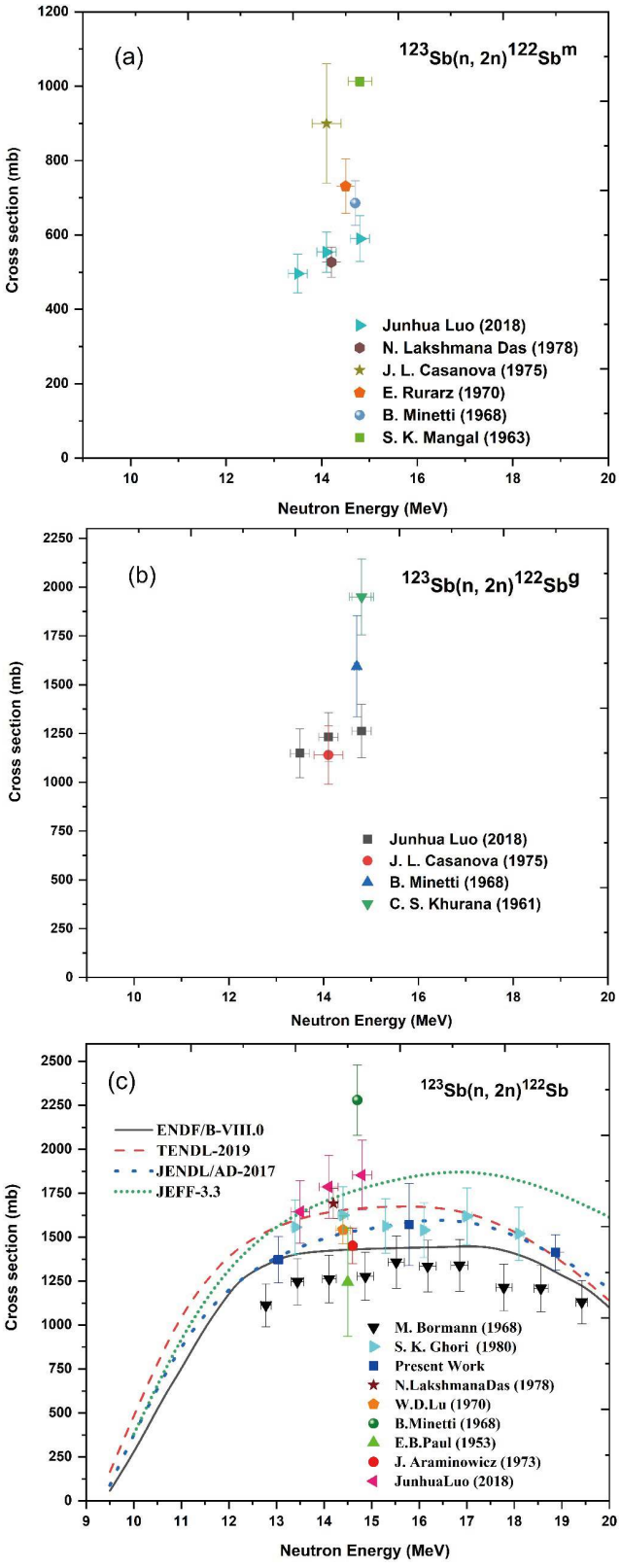

Fig. 5. (color online) Comparison of existing literature and evaluated data of the ^{123}Sb$(n,2n)^{122}$Sb^{m}, ^{123}Sb$(n,2n)^{122}$Sb^{g} and ^{123}Sb$(n,2n)^{122}$Sb reactions.

^{121}Sb$(n,2n)^{120}$Sb reaction. In addition, the JENDL/AD-2017 and TENDL-2019 evaluations agree with the reported data of J. H. Mccrary *et al.* [63] and Y. Kanda [65] at higher energies within experimental uncertainties. The cross section predicted by the JEFF-3.3 library is too large in the 15 MeV energy region and agrees very well with lower energy data of N. L. Das *et al.* [54], B. Minetti *et al.* [57] and M. Bormann *et al.* [59].

It is observed that, for the ^{123}Sb$(n,2n)^{122}$Sb^{m} and ^{123}Sb$(n,2n)^{122}$Sb^{g} reactions, experimental data exist within 13 –16 MeV neutron energies. The reported experimental results of J. L. Casanova [62], E. Rurarz *et al.* [72] and S. K. Mangal *et al.* [73] are slightly higher than N. L. Das *et al.* [54] and J. Luo *et al.* [61] for the isomeric state. However, the data of J. Luo *et al.* [61] is in agreement with N. L. Das *et al.* [54] as shown in Fig. 5(a). Similarly, we can see from Fig. 5(b) that for the ground state, the results of B. Minetti *et al.* [57] and C. S. Khurana *et al.* [70] are slightly higher than the J. Luo *et al.* [61] and J. L. Casanova [62]. However, the results of J. Luo *et al.* [61] are consistent with J. L. Casanova [62] within experimental error.

From Fig. 5(c), we can be seen that in the 13 to 19 MeV energy range our data at 12.50, 15.79 and 18.87 MeV are consistent with the result of the JENDL/AD-2017 evaluation for the ^{123}Sb$(n,2n)^{122}$Sb reaction. At 15.79 and 18.87 MeV, the present measured data are in agreement with the results of the TENDL-2019 evaluation, whereas at 12.50 MeV the present measurement data are in agreement with the ENDF/B-VIII.0 evaluation, as we can see from Fig. 5(c). However, the results of W. D. Lu *et al.* [55] and S. K. Ghorai *et al.* [56] are in agreement with the result of the JENDL/AD-2017 evaluation within experimental uncertainties. Similarly, the results of N. L. Das *et al.* [54] and J. Luo *et al.* [61] agree very well with the JEFF-3.3 evaluation.

V. CROSS SECTION SEMI-EMPIRICAL FORMULAE AND RESULTS SYSTEMATIC FORMULAE

The different semi-empirical formulae for calculating neutron-induced reaction cross sections such as $(n,p),(n,2n),(n,\alpha)$ and (n,t) reactions are developed by various authors for incident neutron energies around 14 to 15 MeV. The experimental cross section of neutron-induced reactions is given by the relation,

$$\sigma(n,x) = C\sigma_{ne}e^{as}, \tag{13}$$

where C and a are the fitting parameters for different reactions obtained by the least square method, s is the asymmetry parameter $s=(N-Z)/(A)$ and σ_{ne} is the non-elastic cross section. These non-elastic cross sections have been measured for many nuclei, varying with the atomic mass of the nuclei. The semi-empirical formulae for the $(n,2n)$ cross section developed by the authors Chatterjee [28], Lu and Fink [29], Luo [30], Bychkov [31] and Habbani [32] within 14 to 15 MeV energies are given in Table 10. All semi-empirical formulae developed by various authors are exponentially dependent on the mass number A, the neutron number N and proton number Z of the target nucleus. We have calculated neutron-induced $(n,2n)$ reaction cross sections for the ^{121}Sb and ^{123}Sb isotopes from systematic formulae, and calculated values are given in Table 11. The cross section data from these formulae are essential in nuclear reaction theories, medical accelerators, and the designing and shielding of advanced reactors.

The cross sections of the ^{121}Sb$(n,2n)^{120}$Sb and ^{123}Sb$(n,2n)^{122}$Sb reactions were calculated from the systematic formulae, and the obtained values are given in Table 11. It is observed that $(n,2n)$ reaction cross sec-

Table 10. Systematic formulae for$(n,2n)$ reaction cross section given by different authors.

Authors	The formulae for $(n,2n)$ cross section	Mass region	Ref.
Chatterjee	$\sigma_{n,2n}=31.39\left(A^{\frac{1}{3}}+1\right)^2\exp\left(\frac{1.706(N-Z)}{A}\right)$	45≤ A ≤238	[28]
Lu and Fink	$\sigma_{n,2n}=45.76\left(A^{\frac{1}{3}}+1\right)^2\left[1-7.372\exp\left(\frac{-32.21(N-Z+1)}{A}\right)\right]$	28≤ Z ≤82	[29]
Luo	$\sigma_{n,2n}=0.0226\left(A^{\frac{1}{3}}+1\right)^2\exp\left(\frac{133.86(N-Z)}{A}-\frac{779.47(N-Z)^2}{A^2}+\frac{1500.51(N-Z)^3}{A^3}\right)$	23≤ A ≤209	[30]
Bychkov	$\sigma_{n,2n}=8.7(A+100)\left[1-0.88\exp\left(\frac{-7.95(N-Z)}{A}\right)\right]$	45≤ A ≤238	[31]
Habbani	$\sigma_{n,2n}=23.53\left(A^{\frac{1}{3}}+1\right)^2\exp\left(3.5\frac{(N-Z)}{A}\right)$	45≤ A ≤209 Odd A	[32]
	$\sigma_{n,2n}=20.82\left(A^{\frac{1}{3}}+1\right)^2\exp\left(3.76\frac{(N-Z+1)}{A}\right)$	48≤ A ≤238 Even A	[32]

Table 11. The$(n,2n)$ reaction cross sections for ^{121}Sb and ^{123}Sb isotopes estimated using systematic formulae.

Authors	^{121}Sb$(n,2n)^{120}$Sb	^{123}Sb$(n,2n)^{122}$Sb
Chatterjee	1410	1458
Lu and Fink	1519	1569
Luo	1568	1626
Bychkov	1369	1440
Habbani	1360	1442
JENDL/AD-2017	1471	1533
ENDF/B-VIII.0	1607	1430
TENDL-2019	1524	1659
JEFF-3.3	1621	1709
EXFOR	1364	1853

tions obtained from formulae of Chatterjee and Bychkov agree with literature data of J. H. Mccrary *et al.* [63] and J. Araminowicz *et al.* [64] for the ^{121}Sb$(n,2n)^{120}$Sb reaction, and with data of J. Araminowicz *et al.* [64] for the ^{123}Sb$(n,2n)^{122}$Sb reaction. Similarly, the cross sections obtained from the formulae of Luo and Lu and Fink are in agreement with literature data of Y. Kanda [65] for the ^{121}Sb$(n,2n)^{120}$Sb reaction and data of W. D. Lu *et al.* [55] and S. K. Ghorai *et al.* [56] for the ^{123}Sb$(n,2n)^{122}$Sb reaction. In contrast, the $(n,2n)$ reaction cross sections obtained from the Habbani formulae are much lower compared to other formulae and do not agree with the available literature data of ^{121}Sb and ^{123}Sb isotopes.

VI. THEORETICAL CALCULATIONS

Different theoretical models have been developed in nuclear physics to understand the compound nucleus, pre-equilibrium and direct nuclear reaction mechanisms. Theoretical calculations of the ^{121}Sb$(n,2n)^{120}$Sb^{m}, ^{121}Sb$(n,2n)^{120}$Sb^{g} and ^{121}Sb$(n,2n)^{120}$Sb reactions as well as for the ^{123}Sb$(n,2n)^{122}$Sb^{m}, ^{123}Sb$(n,2n)^{122}$Sb^{g} and ^{123}Sb$(n,2n)^{122}$Sb reactions cross section were performed by the statistical nuclear reaction codes TALYS (ver. 1.9) [13] and EMPIRE (ver. 3.2.2) [14]. In both codes, different nuclear level density, pre-equilibrium models and other input parameters are given, and these parameters were used to calculate the $(n,2n)$ reaction cross sections.

A. EMPIRE (ver. 3.2.2) calculations

In the EMPIRE code, the theoretical calculations of the compound nucleus (CN) particles and γ-ray emission were described by the statistical theory of Hauser–Feshbach [33] and the width fluctuation correction for this neutron-induced reaction was considered using the Hofmann –Richert –Tepel –Weidenmuller (HRTW) model [34]. Different nuclear level density models were chosen to calculate the $(n,2n)$ reaction cross sections. The optical model parameters given by Koning and Delaroche [35] for neutrons and protons were used from the Reference Input Parameters Library (RIPL-3) [36] database. The exciton model code PCROSS developed by Kalbach [37] was used to study the pre-equilibrium contribution in the reaction cross section. Further, the pre-equilibrium contribution in the cross section was obtained by the theories of quantum-mechanical pre-equilibrium models multistep compound (MSC) and multistep direct (MSD) [38–39]. The direct reaction was described by coupled channel calculations using an optical potential (ECIS code in DR). The γ-ray strength function was described by the Brink–Axel model [40–41], except for E1, where the empirical model of Kopecky and Uhl was used for calculation [42]. In EMPIRE code, phenomenological EMPIRE-specific level density (ESLM) [47], Gilbert –Cameron (GCM) [46] and generalized superfluid (GSM) [49, 50] level density models were used for the cross section calculations. The generalized superfluid model used BCS theory in the low energy region and the Fermi-gas model (FGM) in the high energy region. The Gilbert–Cameron nuclear level density model utilized the constant temperature model (CTM) in the low energy region and the FGM in the high energy region. The generalized superfluid model includes deformation effects by an empirical parameter δ considered in the moment of inertia. The third level density based on the Hartree –Fock Bogoliubov microscopic model (HFBM) was also used for cross section estimation [53].

B. TALYS (ver. 1.9) calculations

Furthermore, calculations with statistical nuclear reaction code TALYS (ver. 1.9) [12] were performed to analyse and predict nuclear reactions. This code simulates the nuclear reactions that involve neutrons, protons, photons, deuterons, tritons and α-particles in the energy range from 1 keV to 200 MeV with mass of target nuclei 12 and heavier. The CN cross section was calculated considering the Hauser –Feshbach theory [33] and default Moldauer model [43– 44], including width fluctuation correction in reactions. The Koning and Delaroche [35] phenomenological optical model local potential was used in the theoretical cross section calculations. The exciton model of Koning and Duijivestjin [45] was used to study the pre-equilibrium contribution in the reaction cross section. The γ-ray strength function (SF) was described by the Kopecky–Uhl generalized Lorentzian [42]. In the TALYS code, six different nuclear level density models are given and used for predicting the cross section at excitation energies where discrete level information is unavailable or incomplete. These models range from phenomenological analytical expressions to tabulated level densities derived from microscopic models. Three phenomenological level densities were suggested. The first is the constant temperature model (CTM) introduced by Gil-

bert and Cameron [46]. In this model, denoted 'ldmodel 1', the excitation energy divided into two parts: a lower energy region where the constant temperature law is applied and a higher energy region where the Fermi gas model is applied. 'ldmodel 2' is the back-shifted Fermi gas model (BFGM) [47], in which the Fermi gas expression is used in all energy region. 'ldmodel 3' is the generalized superfluid model (GSM), which considers superconductive pairing correlations according to the theory of the Barden–Cooper–Schrieffer — i.e., at low energy, paring correlations strongly influence the level density, and the high energy region is described by the Fermi gas model [48–50]. Similarly, three microscopic level density models were also suggested in the TALYS code. In 'ldmodel 4', for the RIPL database, S. Goriely has calculated level densities from drip line to drip line based on Hartree–Fock calculations for excitation energies up to 150 MeV and for spin values up to $I = 30$ [51]. In 'ldmodel 5', the calculations make coherent use of nuclear structure properties determined within a deformed Skyrme–Hartree–Fock Bogolyubov framework. Level densities for more than 8500 nuclei are made available in tabular format for excitation energies up to 200 MeV and for spin values up to $J = 49$ [52]. 'ldmodel 6' is based on temperature-dependent Hartree–Fock Bogolyubov calculations using the Gogny force [53]. The relative feeding of the isomeric and ground states can be used as a 'probe' to investigate the spin distribution of the populated excited states of the compound nucleus. The spin cut-off parameter σ_F^2 represents the width of the angular momentum distribution of the level density and is given by the following equation,

$$\sigma_F^2(E_x) = 0.01389(A^{5/4}/\widehat{\alpha})\sqrt{\alpha U}\,, \tag{14}$$

where A is the mass number, U is the effective excitation energy defined as $U = (E_x - \Delta)$, E_x is the true excitation energy and the energy shift Δ is an empirical parameter that is equal to, or for certain models, closely equivalent to, the pairing energy that is used to represent observed odd–even effects in nuclei. The parameter α is the energy-dependent level density parameter, which considers shell effects at low energies and the damping at higher excitation energy. When shell effects are absent, the parameter $\widehat{\alpha}$ is called the asymptotic level density parameter and is equal to the α parameter. The TALYS keyword "Rspincut" was modified (from the default value of 1.0) to reproduce the existing experimental data. This keyword represents a multiplication factor of the spin cut-off parameter σ_F^2.

C. Theoretical calculation results

Statistical calculations were performed by the TALYS (ver. 1.9) and EMPIRE (ver. 3.2.2) codes using different level density and pre-equilibrium models. The experimental data obtained in the present work are discussed and compared with the literature data and results from the available evaluations: the TENDL-2019, JEFF-3.3, JENDL/AD-2017, and ENDF/B-VIII.0 databases. Due to the very small cross section of the (n,γ) reaction above the 9 MeV energy region, the small contribution to the γ-ray activity of products from the ^{121}Sb$(n,\gamma)^{122}$Sb reaction can be neglected. In the present work, further study of the existing experimental cross section data for populating ^{120}Sb and ^{122}Sb ground and isomeric state as well as the total were also discussed and compared with the theoretical calculations obtained from the TALYS (ver. 1.9) and EMPIRE (ver. 3.2.2) codes.

1. $^{121}Sb(n,2n)^{120}Sb^{m}$, $^{121}Sb(n,2n)^{120}Sb^{g}$ and $^{121}Sb(n,2n)^{120}Sb$ reactions

The theoretical calculations from the TALYS and EMPIRE codes utilizing different level density models were performed for the ^{121}Sb$(n,2n)^{120}$Sb^{m}, ^{121}Sb$(n,2n)^{120}$Sb^{g} and ^{121}Sb$(n,2n)^{120}$Sb reactions and results are demonstrated in Fig. 6 from threshold to 26 MeV neutron energies. Different statistical models were used in the TALYS and EMPIRE codes for the estimation of cross sections, and these models are included in Tables 12 and 13.

It can be seen that for the isomeric state the theoretical TALYS calculations based on three phenomenological level density models are in agreement with the results of N. L. Das *et al.* [54] and W. D. Lu *et al.* [55]. However, our results at 12.50, 15.79 and 18.87 MeV and reported data [56–59] are much higher than those of the three phenomenological models for the ^{121}Sb$(n,2n)^{120}$Sb^{m} reaction. The three phenomenological level density models for the ^{121}Sb$(n,2n)^{120}$Sb^{g} reaction are able to reproduce the reported experimental data very well within the experimental uncertainties.

The TALYS calculations using microscopic level density models Goriely and Goriely–Hilaire for the ^{121}Sb$(n,2n)^{120}$Sb^{m} reaction are able to reproduce the experimental data of S. K. Ghorai *et al.* [56], B. Minetti *et al.* [57] and R. Pepelnik *et al.* [58], within experimental uncertainties. It can be seen that, in the 13 to 18 MeV energy range, the results of S. K. Ghorai *et al.* [56] and M. Bormann *et al.* [59] are consistent with the results of TALYS calculations using the microscopic level density model Goriely–Hilaire–Gogny for the isomeric state, whereas for the ground state the Goriely and Goriely–Hilaire level density models calculations are in agreement with the existing experimental data. In addition, for the isomeric state the TALYS calculation using microscopic level density model Goriely–Hilaire–Gogny overestimated the cross section and agreed with the lower energies data of S. K. Ghorai *et al.* [56] and M. Bormann *et al.*

Table 12. Models and parameterization of the TALYS (ver. 1.9) code used to calculate $(n,2n)$ reaction cross section of ^{121}Sb and ^{123}Sb isotopes.

Optical model	Level density models	Pre-equilibrium models	$E1$ γ-ray strength function model
Koning–Delaroche local OMP	Constant temperature model Back-shifted Fermi gas model Generalized superfluid model Goriely (microscopic model 1) Goriely–Hilaire (microscopic model 2) Goriely–Hilaire–Gogny force (microscopic model 3)	preeqmode 2	Kopecky–Uhl generalized Lorentzian

Table 13. Models and parameterization of the EMPIRE (ver. 3.2.2) code used to calculate $(n,2n)$ reaction cross section of ^{121}Sb and ^{123}Sb isotopes.

Optical model	Level density models	Pre-equilibrium models	$E1$ γ-ray strength function model
Koning global potential	Constant temperature model (GCM) Generalized superfluid model (GSM) Hartree–Fock–Bogoliubov model (HFBM)	Exciton model calculations with code PCROSS, quantum-mechanical pre-equilibrium models multistep compound (MSC) and multistep direct (MSD)	Phenomenological Brink–Axel model

[59]. In contrast, for the ^{121}Sb$(n,2n)^{120}$Sb^{g} reaction, this model underestimated the cross section within neutron energies from 11 to 22 MeV, and agreed only with R. A. Jarjis [60] at 16 MeV energies. The TALYS calculations using microscopic level density model Goriely for the isomeric state and phenomenological level density model back-shifted Fermi gas for the ground state show overall agreement with the present work and existing data, as shown in Figs. 6(a) and 6(b).

Furthermore, our results at 12.50, 15.79 and 18.87 MeV energies agree very well with the EMPIRE calculation using the ESLD level density model as plotted in Fig. 6(a). However, the results of EMPIRE calculations using the GSM, GCM and HFBM level density models are in agreement with the reported data within experimental uncertainties for the ^{121}Sb$(n,2n)^{120}$Sb^{m} reaction. Similarly, the EMPIRE calculation using the GCM level density model describes the data reasonably well for the ground state, as shown in Fig. 6(b). In contrast, the experimental results of the ^{121}Sb$(n,2n)^{120}$Sb^{g} reaction are in agreement with the ESLD and HFBM models calculations, whereas the GSM model calculation agrees with the reported data. The measurements of the various experimenters agree very well with each other except for some of the measurements reported by R. A. Jarjis [60] and C. Carles [69] for the ^{121}Sb$(n,2n)^{120}$Sb^{g} reaction.

However, for the results of the ^{121}Sb$(n,2n)^{120}$Sb reaction, the theoretical calculations from the TALYS code based on the generalized superfluid and back-shifted Fermi gas models describe the data of J. H. Mccrary *et al.* [63], J. Araminowicz *et al.* [64], and the data of Y. Kanda [65] within the 13 to 14 MeV energy range. In contrast, the constant temperature model is able to describe the data of Y. Kanda [65] within the 14 to 15 MeV energy range, the data of J. H. Mccrary *et al.* [63] at 15.34 MeV and the lower-energy data of M. Bormann *et al.* [59]. In addition, the TALYS calculations based on the microscopic models agree very well with J. H. Mccrary *et al.* [63], J. Araminowicz *et al.* [64], and the data of Y. Kanda [65] within the 13 to 14 MeV energy range. The TALYS calculation using the Goriely–Hilaire–Gogny microscopic model is plotted in Fig. 6(c).

Furthermore, the EMPIRE calculation using the GSM is able to describe the data of N. L. Das *et al.* [54], M. Bormann *et al.* [59] for the ^{121}Sb$(n,2n)^{120}$Sb reaction. In contrast, the EMPIRE calculations using the GCM and microscopic HFBM are able to describe the data of Y. Kanda [65] at 14.05 and 14.72 MeV and data of M. Bormann *et al.* [59] from 12.78 to 19.42 MeV energies within experimental uncertainties. The EMPIRE calculation using the GCM level density model describes the reported data as shown in Fig. 6(c).

The contribution of the cross sections from different reaction processes in the ^{121}Sb$(n,2n)^{120}$Sb reaction were studied from threshold to 30 MeV neutron energies. It is observed that the contribution of the pre-equilibrium process increases with energy above 19 MeV. The contribution from the direct process is zero in reaction cross section and the compound nucleus process contributes maximum cross section. The more significant pre-equilibrium emission leads to a reduction in the compound nucleus emission. In order to investigate the effect of the pre-equilibrium emission at higher energies, theoretical calculations were performed using the EMPIRE code. Therefore, a more detailed comparison of the EMPIRE calculations using different pre-equilibrium and level density models for the ^{121}Sb$(n,2n)^{120}$Sb reaction are illustrated in Fig. 6(c). In the present work, the two quantum-mechanical pre-equilibrium models (i) Multi-Step Compound (MSC), and (ii) Multi-Step Direct (MSD) were used to

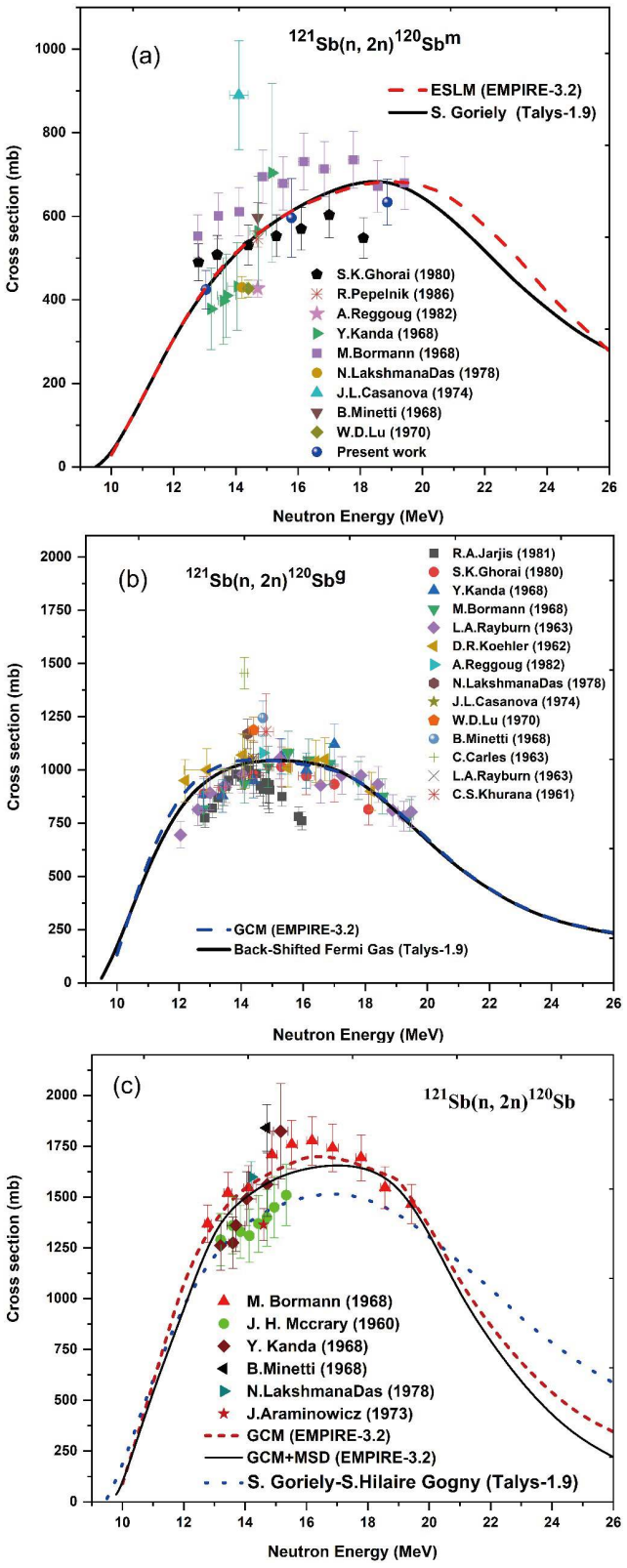

Fig. 6. (color online) Experimental data of the ^{121}Sb$(n,2n)^{120}$Sb^{m}, ^{121}Sb$(n,2n)^{120}$Sb^{g} and ^{121}Sb$(n,2n)^{120}$Sb reactions and theoretical calculations from the TALYS and EMPIRE codes using different level density models.

study the pre-equilibrium emission from the EMPIRE code along with generalized superfluid, Gilbert–Cameron and Hartree–Fock level density models. However, the results of the ^{121}Sb$(n,2n)^{120}$Sb reaction, the MSC pre-equilibrium model with a generalized superfluid, Gilbert–Cameron and Hartree–Fock level density models describe the data of M. Bormann *et al.* [59] up to 16 MeV. In contrast, the MSD pre-equilibrium model with a generalized superfluid, Gilbert–Cameron and Hartree–Fock level density models agree very well with the lower-energy data of the N. L. Das *et al.* [54], M. Bormann *et al.* [59] and Y. Kanda [65]. The best theoretical excitation curve for the ^{121}Sb$(n,2n)^{120}$Sb reaction with the MSD pre-equilibrium and the Gilbert–Cameron level density model is plotted in Fig. 6(c).

2. $^{123}Sb(n,2n)^{122}Sb^{m}$, $^{123}Sb(n,2n)^{122}Sb^{g}$ and $^{123}Sb(n,2n)^{122}Sb$ reactions

The existing experimental data of the ^{123}Sb$(n,2n)^{122}$Sb^{m}, ^{123}Sb$(n,2n)^{122}$Sb^{g} and ^{123}Sb$(n,2n)^{122}$Sb reactions and the theoretical calculations from the TALYS and EMPIRE codes using different level density models are illustrated in Fig. 7 from threshold to 26 MeV neutron energies. The different statistical models used in the calculations are included in Tables 12 and 13.

It is observed that cross section for the isomeric state, the theoretical calculations from TALYS based on the three phenomenological level density models fail to reproduce the experimental data. In contrast, the TALYS calculations using three microscopic level density models are agree very well with the experimental data reported by J. Luo *et al.* [61] and N. L. Das *et al.* [54]. The microscopic calculation based on the Goriely –Hilaire – Gogny model is plotted in Fig. 7(a).

However, for the cross section of the ^{123}Sb$(n,2n)^{122}$Sb^{g} reaction, the TALYS calculation based on the constant temperature level density model is less satisfactory for the literature data of J. Luo *et al.* [61] but agrees very well with the J. L. Casanova [62] for the default value 1.0 for the 'Rspincut' parameter. By reducing the value of 'Rspincut' to 0.6, this model is in agreement with the higher-energy data of J. Luo *et al.* [61] as shown in Fig. 7(b). However, the results of TALYS calculations using the back-shifted Fermi gas and generalized superfluid level density models are lower than the experimental results. In addition, the TALYS calculations using three microscopic level density models fail to describe the experimental data for the ground state.

The EMPIRE calculation using the ESLM level density model describes the ^{123}Sb$(n,2n)^{122}$Sb^{g} reaction cross section reasonably well, as shown in Fig. 7(b). In contrast, the theoretical values from the EMPIRE using the GCM, GSM and HFBM level density models are much higher than experimental values. The reported cross sec-

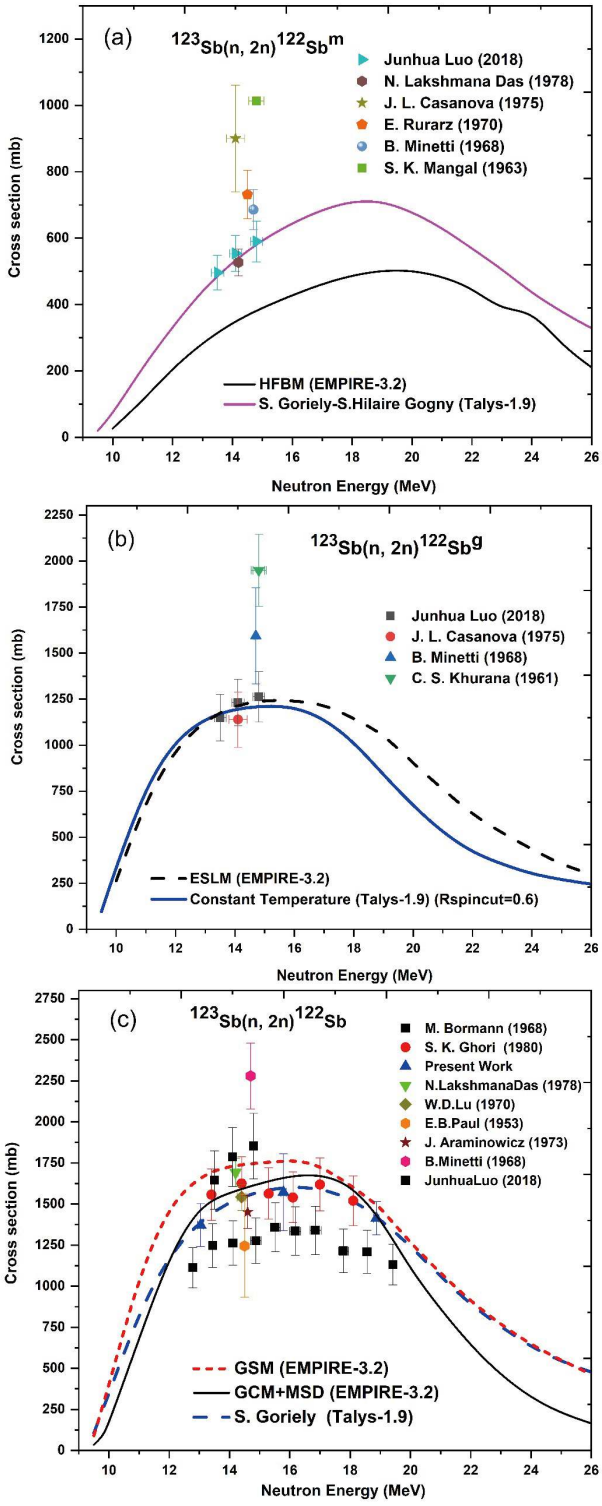

Fig. 7. (color online) Experimental data of the ^{123}Sb$(n,2n)^{122}$Sb^{m}, ^{123}Sb$(n,2n)^{122}$Sb^{g} and ^{123}Sb$(n,2n)^{122}$Sb reactions and theoretical calculations from the TALYS and EMPIRE codes using different level density models.

tions of the ^{123}Sb$(n,2n)^{122}$Sb^{m} reaction are much higher than those of the theoretical excitation curves from the EMPIRE code using the GCM, GSM and HFBM level density models. The results of the EMPIRE calculation using the HFBM model is plotted in Fig. 7(a).

The measured cross sections for the ^{123}Sb$(n,2n)^{122}$Sb reaction at neutron energies of 12.50, 15.79 and 18.87 MeV and the results of the TALYS and EMPIRE calculations using different level density models are plotted in Fig. 7(c), and measured values are given in Table 3. The theoretical calculations from the TALYS code based on the phenomenological level density models describe the data of W. D. Lu *et al.* [55], and S. K. Ghorai *et al.* [56] within the 15 to 16 MeV energy range. In contrast, the TALYS calculations based on the microscopic level density models Goriely and Goriely–Hilaire agrees very well with W. D. Lu *et al.* [55], and S. K. Ghorai *et al.* [56], whereas the calculations based on microscopic level density model Goriely–Hilaire–Gogny is in agreement with the lower-energy data of M. Bormann *et al.* [59], J. Arminowicz *et al.* [64] and with the higher-energy data of S. K. Ghorai *et al.* [56]. Further, the EMPIRE calculation using the GSM model is shown in Fig. 7(c), and it is observed that the generalized superfluid model is in agreement with J. Luo *et al.* [61]. In contrast, the EMPIRE results of the Gilbert–Cameron and Hartree–Fock level density models are consistent with N. L. Das *et al.* [54] and the lower-energy data of S. K. Ghorai *et al.* [56].

The contribution of the cross sections from different reaction processes in the ^{123}Sb(n, $2n$)^{122}Sb reaction were studied from threshold to 30 MeV neutron energies. It is observed that the contribution of the pre-equilibrium process increases with energy above 19 MeV. The contribution from the direct process is zero in the reaction cross section and the compound nucleus process contributes maximum cross section. The more significant pre-equilibrium emission leads to a reduction in the CN emission. In order to investigate the effect of the pre-equilibrium emission at higher energies, theoretical calculations were performed with the EMPIRE code. Therefore, a more detailed comparison of the EMPIRE calculations using different pre-equilibrium and level density models for the ^{123}Sb$(n,2n)^{122}$Sb reaction are illustrated in Fig. 7(c). In the present work, two quantum-mechanical pre-equilibrium models (i) Multi-Step Compound (MSC) and (ii) Multi-Step Direct (MSD) were used to study the pre-equilibrium emission from the EMPIRE code along with generalized superfluid, Gilbert–Cameron and Hartree–Fock level density models. However, for the results of the ^{123}Sb$(n,2n)^{122}$Sb reaction, the MSC pre-equilibrium model with a generalized superfluid, Gilbert–Cameron and Hartree–Fock level density models are able to describe the data of J. Luo *et al.* [61]. In contrast, the MSD pre-equilibrium model with a generalized superfluid, Gilbert–Cameron and Hartree–Fock level density models agree very well with the data of N. L. Das *et al.* [54], W. D. Lu *et al.* [55] and S. K. Ghorai *et al.* [56] within experimental uncertainties, as shown in Fig. 7(c).

3. *Isomeric cross section ratio*

The isomeric pair ^{120}Sb^{m,g} and ^{122}Sb^{m,g} are formed in the $(n,2n)$ reaction on ^{121}Sb and ^{123}Sb isotopes. The EMPIRE and TALYS codes were used to calculate the isomeric to ground state cross section ratio (σ_m/σ_g) theoretically. This ratio is low at low energies and increases as the incident particle energy increases, resulting in an increase in the population of high spin levels of the compound nucleus. The reported experimental data and theoretical results of the TALYS and EMPIRE calculations based on the different level density models are shown together in Figs. 8(a) and 8(b).

For the isomeric pair ^{120}Sb^{m,g}, theTALYS calculations using three phenomenological level density models are in agreement with the experimental data of W. D. Lu *et al.* [55], Y. Kanda [65] and A. Reggoug *et al.* [66] in the lower-energy region, whereas in the higher-energy region the calculated isomeric cross section ratio retains the trend of underestimating. In contrast, the TALYS calculations based on the microscopic level density models Goriely and Goriely–Hilaire reproduce the higher-energy data of M. Bormann *et al.* [59] and the lower-energy data of S. K. Ghorai *et al.* [56] and Y. Kanda [65] within experimental uncertainties, whereas the microscopic level density models of Goriely–Hilaire–Gogny overestimated the isomeric cross section ratio in higher-energy regions and agreed only with the lower-energy data of M. Bormann *et al.* [59] and J. L. Casanova [62].

However, the theoretical isomeric cross section ratio from the EMPIRE code based on the GSM, GCM and HFBM level density models are in agreement with the S. K. Ghorai *et al.* [56], Y. Kanda [65] and the higher-energy data of M. Bormann *et al.* [59] within experimental uncertainties. The results show that the TALYS and EMPIRE calculations using the GCM and Goriely level density models describe quite well the behaviour of isomeric cross section ratio, as shown in Fig. 8(a).

It can be seen that, for the ^{123}Sb$(n,2n)^{122}$Sb^{m}/^{123}Sb$(n,2n)^{122}$Sb^{g} isomeric cross section ratio, literature data exist only in the energy region 13–15 MeV. The theoretical calculations from the TALYS code based on the three phenomenological level density models are in agreement with the data of B. Minetti *et al.* [57] and J. Luo *et al.* [61]. The results show that the back-shifted Fermi gas model describes the isomeric cross section ratio quite well, as shown in Fig. 8(b). However, the TALYS calculations based on the three microscopic level density models does not reproduce the reported experimental data.

The theoretical excitation curve from the EMPIRE calculation using the HFBM level density model is lower than the data of B. Minetti *et al.* [57], J. Luo *et al.* [61] and J. L. Casanova *et al.* [62], as shown in Fig. 8(b). However, the results of the GCM and GSM level density models does not reproduce the experimental data of the previous work.

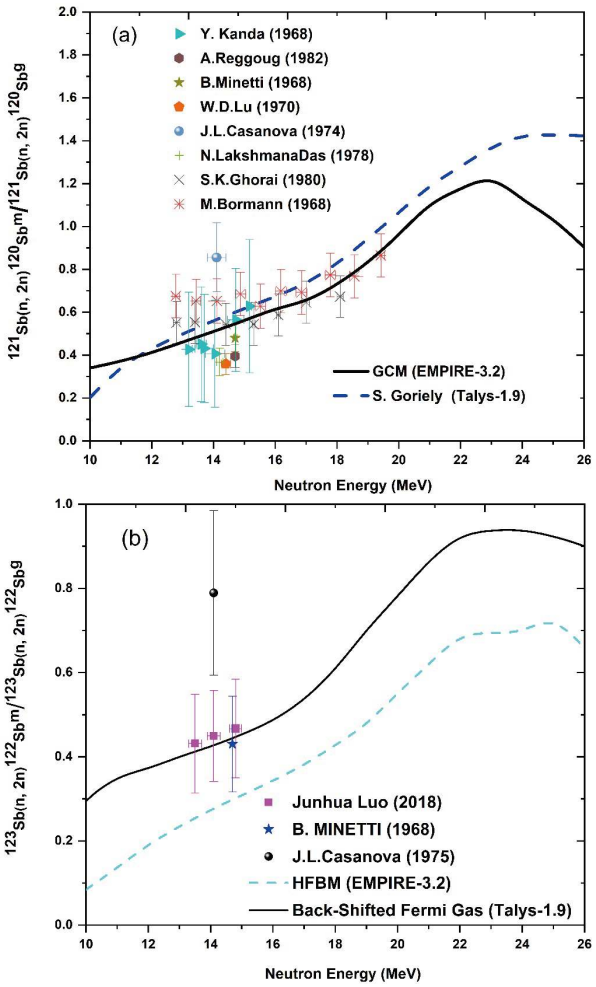

Fig. 8. (color online) Isomeric cross section ratio (σ_m/σ_g) and theoretical calculations from the TALYS and EMPIRE codes using different level density models.

VII. SUMMARY AND CONCLUSIONS

The cross sections for the ^{121}Sb$(n,2n)^{120}$Sb^{m} and ^{123}Sb$(n,2n)^{122}$Sb reactions were measured using the neutron activation and offline γ-ray spectrometric techniques in the 13 –19 MeV energy region relative to the ^{27}Al$(n,\alpha)^{24}$Na reference reaction. The present measured data and statistical cross sections from the TALYS and EMPIRE codes were compared with the previous literature data and evaluated JEFF-3.3, ENDF/B-VIII.0, JENDL/AD-2017 and TENDL-2019 libraries. A detailed analysis of uncertainties in efficiencies of the HPGe detector and present measured cross sections were studied by covariance analysis. In addition, the different authors' formulae were used to systematically study the $(n,2n)$ reaction cross section of antimony isotopes. The formulae of Chatterjee, Bychkov Luo and Lu and Fink reproduce

the cross sections very well except for the Habbani formula. The theoretical calculations of the $(n,2n)$ reaction cross sections for ground and isomeric states and the isomeric cross section ratio were performed using the statistical nuclear reaction codes TALYS (ver. 1.9) and EMPIRE (ver. 3.2.2). The calculated cross sections differ in magnitude only due to different nuclear inputs and different nuclear reaction models in the theoretical calculations. The emission of particles and photons in CN is the dominant reaction mechanism, just above the two-neutron emission threshold energy. The CN cross section depends on the OPs, NLDs, and γSFs statistical nuclear ingratiates. In conclusion, the cross section from the EMPIRE calculations differ only due to the difference between the generalized superfluid and Gilbert–Cameron level density models. This generalized superfluid level density model considered the deformation effect and played an essential role in describing the $(n,2n)$ reaction cross section. We considered nuclear ingratiates OPs, level density, pre-equilibrium and γSFs for comparisons in the EMPIRE and TALYS calculations. It is shown that the two nucleon OPs of Koning and Delaroche give the same results. Similarly, for the γSFs, the phenomenological Brink –Axel model used in EMPIRE and Kopecky–Uhl generalized the Lorentzian model used in the TALYS code. It is safe to say that EMPIRE and the TALYS calculations differ only by using different theoretical models. The TALYS calculations at energies above 14 MeV saturated more rapidly compared to the EMPIRE calculation. It is observed that more experimental data are needed in the high-energy region to investigate the contribution of different reaction channels and to test the reliability of the theoretical calculations. The outcomes of the experiment discussed here will be used for the evaluation of nuclear data libraries, verification of nuclear reaction models, and other basic fundamental applications.

ACKNOWLEDGEMENTS

The authors are thankful to the BARC-TIFR Pelletron accelerator facility staff for their support and help during the experiment. Special thanks to Rohan (BARC-TIFR target lab) for providing Li and Ta targets for the experiment. One of the authors (RKS) is thankful for the IUAC New Delhi financial assistance through a research project (IUAC/XIII.7/UFR-60321).

References

[1] A. J. Koning, J. Blomgren, R. Jacqmin *et al. Nuclear data for sustainable nuclear energy*, JRC Scientific and Technical Reports No. EUR 23977 EN – 2009
[2] N. Otuka, E. Dupont, V. Semkova *et al.*, *Experimental Nuclear Reaction Data Library (EXFOR)*, Nuclear Data Sheets, **120**, 272-276 (2014)
[3] P. Reimer, V. Avrigeanu, S. V. Chuvaev *et al.*, Phys. Rev. C **71**, 044617 (2005)
[4] Keiichi Shibata, Journal of Nuclear Science and Technology **51**, 425-436 (2014)
[5] IAEA Safety Standards Series. Application of the concepts of exclusion, exemption and clearance (No. RSG-1.7). Vienna: International Atomic Energy Agency; (2004)
[6] Vishwanath P. Singh and N. M. Badiger, Indian Journal of Pure & Applied Physics **54**, 443-448 (2016)
[7] Milad Enferadi and Mahdi, Sadeghi Nuc. Tech. & Radia. Prote. **26**(1), 58-63 (2011)
[8] N. Patronis C. T. Papadopoulos, S. Galanopoulos *et al.*, Phys. Rev. C **75**, 034607 (2007)
[9] Arjan Plompen, the JEFF-3.3 Nuclear Data Library, Nov. (2017)..
[10] K. Shibata, N. Iwamoto, S. Kunieda *et al.,* "JENDL/AD-2017" "Activation Cross-section File for Decommissioning of LWRs" JAEA-Conf 2016-004, pp. 47-52
[11] D. A. Brown, M. Herman, A. Trkov *et al.*, "EDNF/B-VIII. 0. " Nuclear Data Sheets **148**, 1-142 (2018)
[12] A. J. Koning, D. Rochman, M. Fleming *et al.*, "TENDL-2019" Nuclear Data Sheets **155**, 1-55 (2019)
[13] A. J. Koning *et al.*, TALYS (ver. 1.9), A Nuclear reaction program, user manual, NRG-1755 ZG Petten, The Netherlands (2018)
[14] M. Herman, R. Capote, B. V. Carlson *et al.*, "EMPIRE (ver. 3.2. 2): Nuclear Reaction Model Code System for Data Evaluation", Nucl. Data Sheets, **108**, 2655-2715 (2007)
[15] J. F. Ziegler, Nucl. Instrum. Methods B **219-220**, 1027 (2004)
[16] C. H. Poppe, J. D. Anderson, J. C. Davis *et al.*, Phys. Rev. C **14**, 438 (1976)
[17] M. W. Mcnaughton, N. S. P. King, F. P. Brady *et al.*, Nuclear Instruments and Methods **130**, 555-557 (1975)
[18] R. B. Firestone, Nucl. Data Sheets **108**, 2319 (2007)
[19] S. Ohya, Nucl. Data Sheets **102**, 547 (2004)
[20] S. Ohya, Nucl. Data Sheets **111**, 1619 (2010)
[21] D. W. Millsap and S. Landsberger, Appl. Radiat. Iso. **97**, 21-433 (2015)
[22] R. Nowotny, XMuDat: Photon attenuation data on PC, IAEA Report IAEA-NDS 195 (1998)
[23] R. Capote, K. I. Zolotarev *et al.*, IRDFF-1.05, Technical Report INDC (NDS)-0616, IAEA, Vienna, (2012)
[24] D. L. Smith, A. J. M. Plompen, and V. Semkova, Correction for low energy neutrons by spectral indexing. Vol. 19 (NEA/WPEC-19, ISBN 92-64-01070-X)
[25] T. Vidmar, EFFTRAN-A Monte Carlo efficiency transfer code for gamma-ray spectrometry, Nucl Instrum Methods Phys. Res. A **550**, 603-608 (2005)
[26] L. P. Geraldo, Nucl. Instrum. And Methods in Phys. Res. A **290**, 499–508 (1990)
[27] N. Otuka, B. Lalremruata, L. R. M. Punte *et al.*, Radiation Physics and Chemistry (2017)
[28] S. Chatterjee and A. Chatterjee, Nucl. Phys. A **125**, 593 (1963)
[29] W. Lu and R. W. Fink, Phys. Rev. C **4**, 1173 (1971)
[30] J. Luo, F. Tuo, F. Zhou *et al.*, Nucl. Instrum. Methods Phys. Res. B **266**, 4862-4868 (2008)

[31] V. M. Bychkov, V. N. Manokhin *et al.*, INDC (CCP)-146, IAEA-NDS, 1980. Vienna, Austria
[32] F. I. Habbani and K. T. Osman, Appl. Radiat. Isot. **54**, 283-290 (2001)
[33] W. Hauser and H. Feshbach, Phys. Rev. **87**, 366 (1952)
[34] H. M. Hofmann, J. Richert, J. W. Tepel *et al*., Ann. Phys. (NY) **90**, 403 (1975)
[35] A. J. Koning and J. P. Delaroche, Nucl. Phys. A **713**, 231 (2003)
[36] R. Capote, M. Herman, P. Oblozinsky *et al.*, "RIPL – Reference Input Parameter Library for Calculation of Nuclear Reactions and Nuclear Data Evaluations" Nuclear Data Sheets **110**, 3107–3214 (2009)
[37] C. Kalbach, Z. Physik A **283**, 401 (1977)
[38] T. Tamura, T. Udagawa, and H. Lenske, Phys. Rev. C **26**, 379 (1982)
[39] H. Nishioka, J. J. M. Verbaarschot, H. A. Weidenmuller *et al*., Ann. Phys. **172**, 67 (1986)
[40] D. M. Brink, Nucl. Phys. **4**, 215 (1957)
[41] P. Axel, Phys. Rev. **126**, 671 (1962)
[42] J. Kopecky and M. Uhl, Phys. Rev. C **41**, 1941 (1990)
[43] P. A. Moldauer, Phys. Rev. C **14**, 764 (1976)
[44] P. A. Moldauer, Nucl. Phys. A **344**, 185 (1980)
[45] A. J. Koning and M. C. Duijvestijn, Nucl. Phys. A **744**, 15 (2004)
[46] A. Gilbert and A. G. W. Cameron, Can. J. Phys. **43**, 1446 (1965)
[47] A. V. Ignatyuk, G. N. Smirenkin, and A. S. Tishin, Sov. J. Nucl. Phys. **21**(3), 255 (1975)
[48] W. Dilg, W. Schantl, H. Vonach, and M. Uhl, Nucl. Phys. A **217**, 269 (1973)
[49] A. V. Ignatyuk, K. K. Istekov, and G. N. Smirenkin, Sov. J. Nucl. Phys. **29**(4), 450 (1979)
[50] A. V. Ignatyuk, J. L. Weil, S. Raman, and S. Kahane, Phys. Rev. C **47**, 1504 (1993)
[51] S. Goriely, F. Tondeur, and J. M. Pearson, Atom. Data Nucl. Data Tables **77**, 311 (2001)
[52] S. Hilaire, M. Girod, S. Goriely *et al.*, "Temperature dependent combinatorial level densities with the D1M Gogny force", (2013)
[53] S. Goriely, S. Hilaire, and A. J. Koning, Phys. Rev. C **78**, 064307 (2008)
[54] N. L. Das, C. V. S. Rao, B. V. T. Rao *et al*., Pramana, **11**(5), 595 (1978)
[55] W. D. Lu, N. Ranakumar, and R. W. Fink, Phys. Rev. C, Nuclear Physics **1**, 350 (1970)
[56] S. K. Ghorai, J. E. Gaiser, and W. L. Alford, J. Phys. G. Nucl. Phys. **6**, 393-399 (1980)
[57] B. Minetti and A. Pasquarelli, Zeitschrift fuer Physik **217**, 83 (1968)
[58] R. Pepelnik, B. Anders, B. M. Bahal *et al*., Report-GKSS-No. 86, E-29, (1986)
[59] M. Bormann, A. Behrend, I. Riehle *et al*., Nuclear Physics Section A **115**, 309 (1968)
[60] R. A. Jarjis, Nuclear Instruments and Methods, **184**(2-3), 439-444 (1981)
[61] J. Luo, Li Jiang, and Long He, Applied Radiation and Isotopes, **140**, 115-120 2018
[62] J. L. Casanova, Report from misc. OECD countries to NEANDC, **140**, 9 (1974)
[63] J. H. Mccrary and I. L. Morgan, Bulletin of the American Physical Society **5**, 246 (1960)
[64] J. Araminowicz, J. Dresler, Inst. Badan Jadr. (Nucl. Res.), Swierk+Warsaw, Repts, **1464**, 14 (1973)
[65] Y. Kanda, Journal of the Physical Society of Japan **24**, 17 (1968)
[66] A. Reggoug, G. Paic, and M. Berrada,, Annual Report **5**, 14 (1982)
[67] E. B. Paul and R. L. Clarke, Canadian Journal of Physics **31**, 267 (1953)
[68] L. A. Rayburn, Physical Review **130**, 731 (1963)
[69] C. Carles, Comptes Rendus **257**, 659 (1963)
[70] C. S. Khurana and H. S. Hans, Nuclear Physics **28**, 560 (1961)
[71] D. R. Koehler, W. L. Alford, Div. of Tech. Info. U. S. AEC Reports, No. 11667 (1962)
[72] E. Rurarz, Z. Haratym, A. Sulik *et al*., Acta Physica Polonica, Part B **1**, 415 (1970)
[73] S. K. Mangal and P. S. Gill, Nuclear Physics **49**, 510 (1963)